Atmospheric Environment 201 (2019) 323–333

Contents lists available at ScienceDirect

Atmospheric Environment

journal homepage: www.elsevier.com/locate/atmosenv

Can formaldehyde contribute to atmospheric new particle formation from sulfuric acid and water?

Chun-Yu Wang[a,b], Shuai Jiang[b], Zhong-Quan Wang[a,b], Yi-Rong Liu[b], Hui Wen[a], Teng Huang[a], Ya-Juan Han[a], Wei Huang[a,b,c,*]

[a] Laboratory of Atmospheric Physico-Chemistry, Anhui Institute of Optics & Fine Mechanics, Chinese Academy of Sciences, Hefei, Anhui, 230031, China
[b] School of Information Science and Technology, University of Science and Technology of China, Hefei, Anhui, 230026, China
[c] Center for Excellence in Urban Atmospheric Environment, Institute of Urban Environment, Chinese Academy of Sciences, Xiamen, Fujian, 361021, China

ARTICLE INFO

Keywords:
New particle formation
Formaldehyde
Flow tube reactor
Cluster dynamics model
Cluster growth flux

ABSTRACT

Though sulfuric acid and ammonia/alkyl amines are recognized as main contributors to new particle formation (NPF), models and observations have indicated that other organic species may be involved. In this study we introduced a suitable flow tube system to investigate the effect of formaldehyde (CH_2O) on NPF from sulfuric acid and water at 297 K. Our results showed that nucleation rates are slightly enhanced when adding CH_2O of 0.31–2.40 ppbv (in the range of atmospheric CH_2O peak concentration) to stable sulfuric acid and water system at relative humidity (RH) of 30%, i.e., a rise of the particle number only by a factor of about 2, which is small in comparison to the millionfold increase caused by methylamine in similar conditions. And the promoting effect was weak under different RH. Cluster growth flux at experimental conditions, obtained from quantum chemistry-based cluster evaporation rate constants applied in a cluster population dynamics model, showed H_2SO_4-CH_2O-based clusters are hard to grow. Therefore, the effect of CH_2O on NPF via directly involving in the nucleation can be eliminated. In addition, the derived information may provide new insight into the impact of aldehydes on NPF.

1. Introduction

Aerosol particles in the atmosphere have potential impact on human health and strongly influence the transfer of radiant energy and the spatial distribution of latent heating through the atmosphere, thereby influencing the weather and climate (IPCC, 2013; Nel, 2005; Oberdörster et al., 1992). New particle formation (NPF) takes place in various atmospheric environments from the boundary layer to the upper troposphere and lower stratosphere, and from rural biogenic environments to extremely polluted industrial plumes (Kanawade et al., 2012; Kerminen et al., 2018). The first step of new particle formation or any first order phase transition is nucleation, one of the least understood micro-physical processes in the atmosphere. The chemical composition of the molecular clusters and nanoparticles at nucleation-mode remains highly uncertain despite recent advances in theory and instrumentation (Almeida et al., 2013; Kerminen et al., 2018; Schobesberger et al., 2013).

Nucleation between sulfuric acid (SA) and H_2O has been well studied and serves as a useful point of comparison (Duplissy et al., 2016; Zollner et al., 2012), yet it cannot explain observations (Kanawade et al., 2014; Kerminen et al., 2018; Kuang et al., 2008; Weber et al., 1996; Yao et al., 2018) in the atmospheric boundary layer. In the lower atmosphere, other species, organic vapors as the most plausible alternative (Kürten et al., 2016; Kurtén et al., 2008; Laaksonen et al., 2008; Metzger et al., 2010; Riccobono et al., 2014) must participate to stabilize SA particles. Based on acid-base theory, nitrogenous bases are known to enhance sulfuric acid particles formation via quantum chemical calculations (Nadykto et al., 2011; Ortega et al., 2012) and several experimental studies (Almeida et al., 2013; Ball et al., 1999; Benson et al., 2011; Berndt et al., 2014; Jen et al., 2016; Kürten et al., 2016; Zollner et al., 2012). However, nucleation of H_2SO_4 and H_2O with ammonia or amines often does not reproduce NPF measurements (Kirkby et al., 2011). Such discrepancies between NPF models and observations suggest that other species are involved and may contribute significantly at locations where nitrogenous bases are sparse.

Jang and co-workers performed a series of smog chamber and flow tube experiments to study particle growth, and conclude that reactions of various aldehydes can remarkably increase the secondary organic

* Corresponding author. Laboratory of Atmospheric Physico-Chemistry, Anhui Institute of Optics & Fine Mechanics, Chinese Academy of Sciences, Hefei, Anhui, 230031, China.
E-mail address: huangwei6@ustc.edu.cn (W. Huang).

https://doi.org/10.1016/j.atmosenv.2018.12.057
Received 24 August 2018; Received in revised form 23 November 2018; Accepted 25 December 2018
Available online 10 January 2019
1352-2310/

aerosol mass production (Jang et al., 2003, 2005). The gas-phase concentration of formaldehyde (CH_2O), one of the most abundant carbonyls, ranges from thousands of pptv to dozens of ppbv observed in different area of the world (Possanzini et al., 2002; Wang et al., 2010; Zheng et al., 2013). It is widely concerned because it is an important intermediate product of photochemical reaction in the atmosphere, and it has a certain role in the atmospheric reactivity and oxidizing ability (Anderson et al., 1996; Fried et al., 1997; Grosjean, 1982; Iraci and Tolbert, 1997). It has high reactivity, and is one of the major pollutants in the urban atmosphere. Globally, the main source of formaldehyde in clean and remote areas is the photochemical oxidation of CH_4, but in rural areas, the oxidation of hydrocarbons emitted by natural sources (such as terpenes and isoprene) and man-made sources is also a source of CH_2O (Zimmerman et al., 1978). Previous investigations have suggested that the major sink processes of CH_2O in gas-phase atmospheric chemistry are photolysis (Carbajo et al., 2008; Feilberg et al., 2005) and reaction with the hydroxyl radical (Alvarez-Idaboy et al., 2001), which produces HO_X radicals (Atkinson, 2000; Hak et al., 2005). Budget analyses of CH_2O reveal large discrepancies between observed CH_2O concentrations and those predicted from models (Jacob, 2000; Wagner et al., 2002). Recently, gas phase hydrolysis of CH_2O (Hazra et al., 2013; Liu et al., 2015; Long et al., 2013), uptake of CH_2O by aerosols/clouds (Fried et al., 2003; Tie et al., 2001; Zhou et al., 1996), soil surfaces (Li et al., 2016), and direct participation of CH_2O in nucleation (Shi et al., 2018) are of great interest, which could present additional CH_2O sink pathways and thus reduce overestimation of CH_2O (Wagner et al., 2002). Atmospheric CH_2O can participate in various reactions, such as hydration, aldol condensation, hemiacetal/acetal formation. (Barsanti and Pankow, 2004) α-dicarbonyls such as glyoxal and methylglyoxal are significantly reactive in the particle nucleation processes via hydration reaction or aldol condensation (Zhang et al., 2012). So, understanding the interactions of CH_2O and these products with nucleation precursors may help to delineate the mechanism of NPF and explain the discrepancies of CH_2O.

Described here was a combination of experimental and theoretical studies of new particle formation from mixtures of SA, H_2O and CH_2O. Based on previous techniques (Ball et al., 1999; Zollner et al., 2012), experiments address particle concentrations that result from the combination of all dynamic processes involving the clusters and vapor molecules. Quantum chemistry-based cluster evaporation rate constants are applied in a cluster population dynamics model to yield cluster formation rates. How CH_2O can influence the nucleation process on new particle formation of the sulfuric acid-water system was investigated in this study. However, because the molecular composition of nucleating clusters was not measured with mass spectrometer (Almeida et al., 2013; Schobesberger et al., 2013), which could remove the ambiguity of the role of CH_2O or contaminant on NPF at the molecular level, thus, more experimental work is needed before defining a clear conclusion about the nucleation mechanisms.

2. Experimental and theoretical methods

2.1. Experimental setup

Similar to Ball et al. (1999) the flow system built recently is capable of both binary and ternary homogeneous nucleation measurements. The silicate glass laminar flow tube is positioned horizontally with a total length of ~160 cm and a 4.50 cm ID represented schematically in Fig. 1. Two separate temperature-regulated waters flowing in two jackets were used to control temperature of the two regions: a mixing region near the front where gas and reactants entered (~20 cm long, ~314 K) and a 110 cm long nucleation region (~297 K) with five outlets evenly distributed. The two jacketed flow tubes are joined in a ~18 cm room temperature (298 K) transition section. Formaldehyde was added to the flow tube through an ~2 mm ID port located in the transition region.

Three lines of gas (Q_1, Q_2 and Q_3) were controlled by high precision mass flow controllers (Sevenstar D07-19B) and were regularly calibrated by soap film flowmeter (Gilibrator 2). Dry compressed air was passed through a purge air generator (AADCO 737–15), and a 1 μm combined with a 0.01 μm filter (T-001 and A-001; Jiamei Filters) for further purification. Dry, purified and particle-free air served as the carrier gas in this study. The total mixing gas flow was about 6 L per minute (lpm; 297 K and 0.98atm).

H_2O was introduced by directing a portion of the carrier gas over one water reservoir and then through water in a water bubbler at room temperature for humidification, and finally measured in the nucleation region with a humidity and temperature probe (± 0.5 °C and ± 3 %RH over 10–30 °C; Vaisala HMP60). To remove any amine or ammonia vapor that may come from the ultrapure water (resistivity 18.25 MΩ cm @ 25 °C; KANGNING) or the carrier gas, we added few drops of sulfuric acid (97 wt%; SINOPHARM) to the ultrapure water.

SA was introduced from a liquid reservoir by passing carrier gas through a glass saturator (~30 cm long) filled with high purity H_2SO_4 held at 308 K. The carrier gas flow in the 1/4″ OD Teflon tubing was preheated through a glass reservoir, which used recirculating water flowing after SA saturator. In order to determine the number concentration of gas-phase SA in the tube, the saturation vapor pressure of SA in the saturator was calculated using the following equation: (Kulmala and Laaksonen, 1990)

$$\ln p_{sa} = \ln p_{sa,0} + \frac{\Delta H_v(T_0)}{R}\left[-\frac{1}{T} + \frac{1}{T_0} + \frac{1}{T_c - T_0} \times \left(1 + \ln\frac{T_0}{T} - \frac{T_0}{T}\right)\right] \quad (1)$$

Where p_{sa} is the saturation vapor pressure (atm) of H_2SO_4 at a temperature of T (K), $p_{sa,0}$ is the saturation vapor pressure of H_2SO_4 at the temperature $T_0 = 360$ K, ΔH_v is the enthalpy of vaporization, T is the temperature of the saturator and T_c is the critical temperature ($T_c = 905$ K). Equation (1) is commonly used in studies of H_2SO_4-H_2O or more complex nucleation theories and in their parameterizations. (Merikanto et al., 2007; Vehkamäki et al., 2002) Also, its accuracy has been investigated by Neitola et al. (2015) who reported a comparison of the SA concentrations estimated using Eq. (1) and experimental concentrations measured with online ion chromatograph Monitor for AeRosols and Gases in ambient Air (MARGA; Metrohm Applikon), displaying very good agreement. Skrabalova et al. (2014) has applied it to the flow tube experiment. The SA vapor concentration in the flow tube was then calculated by applying the mixing law. To change the amount of SA, the carrier flow rate that was directed to the bulk SA was varied from 0.3 to 1.0 standard liters per minute. The wall loss of SA in the flow tube was assumed to be a diffusion controlled first-order rate process, which can be described by a simple equation:

$$\ln[H_2SO_4]_L = -k_{obs}L + \ln[H_2SO_4]_0 \quad (2)$$

Where $[H_2SO_4]_0$ is the initial concentration of SA, $[H_2SO_4]_L$ is the concentration after distance L in the flow tube and k_{obs} (cm^{-1}) is the rate constant, which is given by the equation:

$$k_{obs} = \frac{3.65 \cdot D}{r^2 \cdot v} \quad (3)$$

where r is the radius of the flow tube (cm), v is the mean flow velocity in the flow tube (cm s^{-1}), and D is the diffusion coefficient of SA (cm^2 s^{-1}). Here, we use D as 0.089 cm^2 s^{-1}, the simulated result considering only hydrated H_2SO_4 molecules with the CFD-FLUENT model in laminar flow tube at 298 K. (Brus et al., 2017) Fig. 2 shows $\ln[H_2SO_4]$ vs distance in the flow tube for five the carrier flow rate above SA saturator. These are most likely the maximum concentration of sulfuric acid under the condition of 297 K and higher RH, because the determined diffusion coefficients decreased with decreasing temperature (Brus et al., 2017) and increasing RH. (Hanson and Eisele, 2000) It needs to be pointed out that gaseous sulfuric acid vapor can undergo strong clustering due to unavoidably presence of base impurities, such

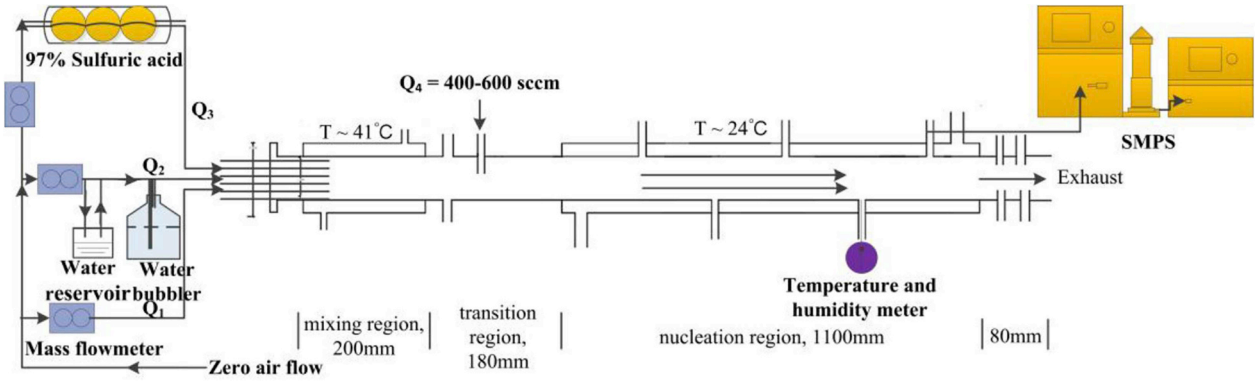

Fig. 1. Diagram of the nucleation flow reactor with mixing, transition and nucleation regions indicated. H_2O source, H_2SO_4 source, the port for the third substance added, the general flow patterns and temperatures are indicated.

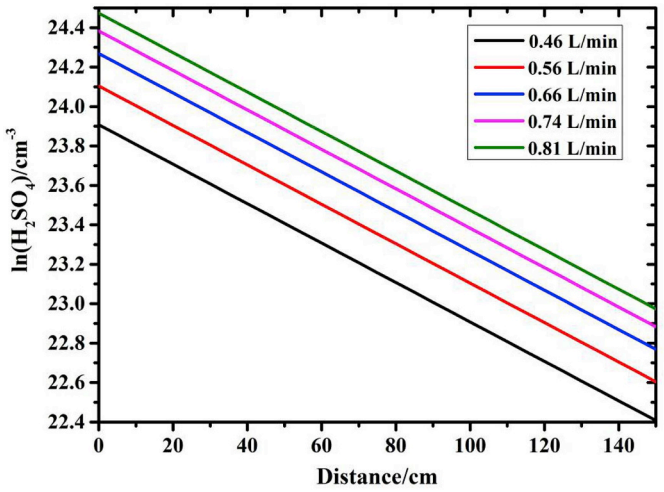

Fig. 2. Simulations of ln[H2SO4] as function of distance in the flow tube under the condition of RH = 4% and T = 298 K.

losses would reduce the H_2SO_4 concentration in the nucleation zone ($[H_2SO_4]_{NZ}$), too.

Gas-phase CH_2O was produced by permeation tube (18 ng/min ± 50% @ 313 K; VICI Metronics) that was kept in permeation chamber of dynacalibrator (VICI Model 500) at a constant temperature of 313 K with a dynamic dilution system using high purity N_2 (≥99.999%). The concentration in the flow tube was calculated via permeation rate of CH_2O and mixing ratios of the flow from the dynamic dilution system and the total flow, assuming no loss to the walls. The series of experiments were started by measuring the H_2SO_4-H_2O system without any additional CH_2O compound. When the particle concentration in the flow tube was stabilized, the CH_2O compound was added, starting from approximately 0.31 to 2.40 ppbv. In order to keep the concentration of sulfuric acid and water constant after the addition of formaldehyde, the decreased flow rate of dry and particle-free air is equal to that of CH_2O added.

Flow tube was cleaned with ultrapure water and purged with dry purified air at least overnight until the particle concentration inside the nucleation chamber drops to near 0 particles cm^{-3}, which is also our background value for pure water. There are always unavoidable impurities of base compounds present in the nucleation reactor or chamber, which is the common issue in nucleation experiments (Almeida et al., 2013; Duplissy et al., 2016; Glasoe et al., 2015; Jen et al., 2014; Kirkby et al., 2011; Merikanto et al., 2016; Yu et al., 2017). Due to the significant effect of bases on nucleation, it is critical to reduce the impurity concentration (Almeida et al., 2013; Glasoe et al., 2015; Jen et al., 2014; Yao et al., 2018). It was found necessary in our experiments to condition the flow reactor with a flow of SA for about 1–3 days to passivate the walls with respect to SA uptake. After this flushing procedure, the impurity concentration of the ammonia (NH_3) dropped drastically and was determined to be below 30 pptv. The earlier studies show that the concentration of ambient gaseous NH_3 is much higher than that of amine by at least two orders of magnitude (Hanson et al., 2011; Qiu and Zhang, 2013; Zheng et al., 2015), meaning that the impurity concentration of amine is below 1 ppt. Impurity measurement in the Supporting Information (SI) describes the offline analytical method of ion chromatography (IC) to quantify the NH_3 impurity concentration.

2.1.1. Particle measurement

The particle size distribution is measured at nearly the end of the nucleation chamber with a scanning mobility particle sizer (SMPS, TSI 3938) comprised of an electrostatic classifier (TSI 3082), a neutralizer (TSI 3088), a nano-differential mobility analyzer (TSI 3085), and a butanol-based ultrafine condensation particle counter (UCPC, TSI 3776). We got a 50% cut-off size of 2.50 nm with the saturator temperature of 39 °C, the condenser temperature of 10 °C in UCPC. While SMPS can detect some particles below 2.50 nm, depending on the composition (Kangasluoma et al., 2014), this portion of the data has high uncertainties and thus was chosen excluded in detection. Size-resolved particle number concentrations were obtained from 2.37 to 80.6 nm every 180 s with SMPS inlet flow of 1.0 lpm. The total particle number concentrations (*Np*) were determined after diffusion losses and the multicharged particles correction. The obtained geometric mean mobility diameters are reported as particle diameters.

The experimental determined nucleation rate (*J*) shown in the present study was estimated by the measured *Np* and dividing nucleation time (t_n shown in Section 2.1.2). Because critical clusters (~1.5 nm) (Kulmala et al., 2007) are typically smaller than the minimum measurable size of the UCPC, the *J* reported here is the so-called "apparent formation rate" (Kerminen and Kulmala, 2002), after which, a large variety of methods have been developed and applied to determine particle formation (Kerminen et al., 2018). Here, with the high concentration of sulfuric acid, the growth rate is so high that the coagulation loses are negligible. The values estimated from such a calculation are close to the actual *J* values.

2.1.2. Particle nucleation time

It is critical and difficult to determine the nucleation time, which is based on nucleation zone from the particles generation to the position where particle losses are equal to the production. Theoretically, the nucleation is a homogeneous process independent on any local changes in vapor-gas mixture composition and temperature. However, the flow profile would be influenced by buoyancy driven convection at the beginning of the nucleation chamber where temperature rapidly changes.

The Richardson number, R_i, quantifies the ratio of natural convection to forced convection. Typically, forced convection is negligible when $R_i > 10$. The Stokes number, S_{tk}, determines whether a particle suspended in a fluid flow will follow the gas streamlines. In this system, the stopping distance calculated for particles from 2 to 20 nm diameter shows that all particles, $S_{tk} \ll 1$, are expected to follow gas streamlines. The distance (~0.03 ReD) for a plug-type flow to attain 95% of the velocity profile of fully developed laminar flow (FDL) is typically ~25 cm, and the Reynolds number, *Re*, for typical conditions was ~200, so that FDL exists in the nucleation region. Though the gas entering the reactor is about 17 K warmer than cooled section of the flow reactor, the laminar flow is fully developed from the beginning of the nucleation chamber, where the temperature of the vapor-gas mixture starts to reach the temperature of inner surface.

Ball et al. (1999) used the nucleation time as 4 s based on a 4 cm s^{-1} flow velocity over the ~15 cm nucleation zone length, then, it was more finely estimated as 8 s taking into account velocity changes in the nucleation zone based on the similar flow tube device which still has a high uncertainty of +100% and −50% (Zollner et al., 2012). Thus, *J*, obtained by dividing *Np* by an estimated nucleation time, also has the high uncertainty. Fig. 3 shows measured particle number versus distance (*L*) from the beginning of the nucleation chamber. This figure should be taken as a qualitative because the raw data were neither continuous nor enough. It shows that the number of particles reached the maximum at ~60 cm from the entrance of reaction tube, where particle losses are equal to the production. So, the nucleation time was estimated to be 10 s (~ ± 17%) assumed that the nucleation is initiated at entrance of nucleation region (~ ± 10 cm). It is important to point out that the nucleation time affects the pre-exponential factor of the experimental nucleation rate but does not affect the power dependencies.

2.2. Theoretical methods

To elucidate the mechanisms of particle formation, structural and thermodynamic information for the global minima of $(CH_2O)_l(H_2SO_4)_m(H_2O)_n$ (l = 1–3, m = 0–3, n = 0–3) clusters were first characterized by the Basin-Hopping structure search algorithm coupled with Density Functional Theory described by Jiang et al. (2014) During this process, the equilibrium structures and enthalpy as well as free energy changes for formation of complexes and small clusters that could lead to particle formation were obtained from PW91PW91/6–311 + + G(3df, 3pd) level of theory, which provides good geometries (Kurtén et al., 2007; Nadykto et al., 2008), excellent vibrational frequencies (Nadykto et al., 2007) and quite accurate cluster free energies compared with the currently available experiments (Nadykto and Yu, 2007; Wang et al., 2018; Wen et al., 2018). A benchmark about the methods employed in atmospheric cluster calculations is available in the SI.

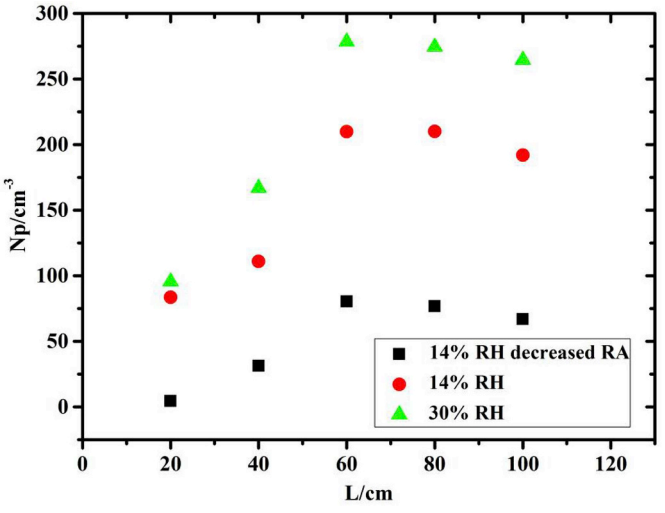

Fig. 3. Measured particle number versus distance (*L*) along the flow reactor for an estimated $[H_2SO_4]_{NZ}$ equal to 1.76×10^{10} cm^{-3} at different RHs. Decreased relative acidity (RA) means that $[H_2SO_4]_{NZ}$ is reduced to 1.26×10^{10} cm^{-3}. The results indicate the region where nucleation occurs in the reactor.

Then, dynamics simulation, based on Atmospheric Cluster Dynamics Code (ACDC) solving the ordinary differential equations (McGrath et al., 2012), was carried out to obtain growth route, which determined by the cluster growth flux (Olenius et al., 2013) as shown in equation (4):

$$F_{(mA.nB)} = \beta_{ij,kl} c_{ij} c_{kl} - \gamma_{ij,kl} c_{mn} \quad (4)$$

Here, $i + k = m$ and $j + l = n$ respectively and F is the cluster growth flux, β is the collision rat efficient in the unit of m^3 s^{-1}, c is the cluster concentration in the unit of m^{-3}, γ is evaporation rate in the unit of s^{-1}. β was calculated according to the kinetic gas theory (Rosenboum, 1941) assuming that all collisions stick, and γ was determined from the quantum chemical Gibbs free energies of formation according to the condition of detailed balance, and more detailed method of calculating the rate coefficient was shown in the study by McGrath et al. (2012) and Ortega et al. (2012).

3. Results and discussion

Even though our study together with previous studies were executed with care and purported to address binary nucleation, most were, to some extent, burdened with ions or ppt level contamination by base impurities like ammonia and amines. The homogeneous nucleation rates as a function of $[H_2SO_4]_{NZ}$ at a constant nucleation temperature of 297 K were determined in this study. Experiments were divided into three types in this study: (1) Changing $[H_2SO_4]_{NZ}$ to stability, (2) Changing relative humidity to stability and (3) Changing CH_2O concentration to stability. Typical experiments are depicted in Fig. 4 where total particle number concentrations are plotted as a function of time. As shown in Fig. 4 (a), when the experiment was started the particle production started to reach a certain plateau value about 2 h, the particle formed stable rapidly after added CH_2O. For increasing H_2SO_4 concentration, the particle production started to be stable in two to 3 h depending on different condition. For increasing RH shown in Fig. 4 (b), the particle production started to be stable in a shorter time depending on different condition. Then, the stable particle production lasts for many hours with a maximum ± 15% change in the total number concentration. The particle number concentration was measured during the whole experiment but assessed only for steady state particle production and subsequently averaged to obtain only one experimental point by 3 samples. The flow tube was very sensitive to any small change in the input parameters (flow rates of sheath and mixing air, temperature of the circular water), which directly lead to changes in the particle production.

3.1. H_2SO_4-H_2O nucleation and comparison to data of other researchers

Recent advanced particle counting methods, including the Particle Size Magnifier (PSM) (Vanhanen et al., 2011), and analytical techniques to determine the relevant H_2SO_4 concentrations, including CIMS (Hanson and Eisele, 2002) and IC (Neitola et al., 2015), have been used in experiments. Despite these advances, the rate data from H_2SO_4-H_2O nucleation flow tube experiments under similar atmospheric boundary layer conditions, illustrated in Fig. 5 (Ball et al., 1999; Benson et al., 2009; Brus et al., 2010, 2011; Sipilä et al., 2010; Young et al., 2008; Yu et al., 2017; Zollner et al., 2012), vary tremendously. Some of the differences stem from impurity levels (base impurities like ammonia and amines or ions produced from cosmic radiation), the method about

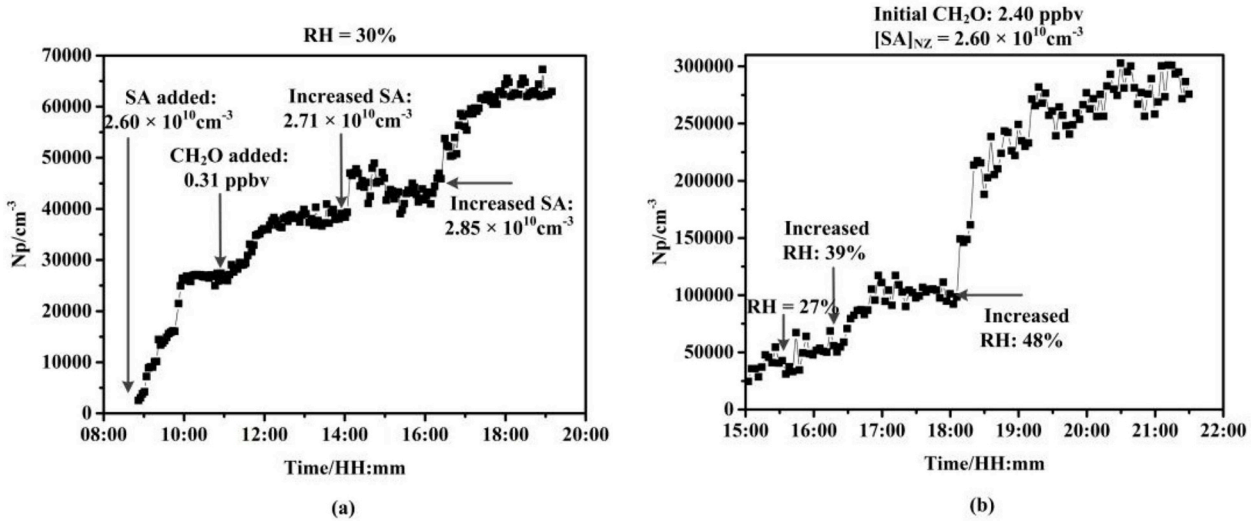

Fig. 4. *Np* plotted versus time for CH_2O addition and increasing $[H_2SO_4]_{NZ}$ to stability at 30% RH (a), and for increasing RH to stability at $[H_2SO_4]_{NZ}$ of $2.60 \times 10^{10}\,cm^{-3}$ with CH_2O concentration of 2.40 ppbv (b).

determining nucleation rates (depend on nucleation zone determination and particle number measurement), and operating conditions including temperature and water vapor concentrations. Among them, Zollner et al. (2012), Yu et al. (2017), and our work measured base impurity levels. Zollner et al. (2012) and our work used concentration of SA in nucleation zone (see SI for comparison on the selection of SA concentration in previous studies). All these experiments used an ultrafine CPC, except that Ball et al. (1999) used an Ultrafine Condensation Nucleus Counter, Sipilä et al. (2010), Brus et al. (2011) and Yu et al. (2017) used a PSM with cutoff diameters more near the critical size. All flow tube experiments here were conducted without removing ions. Duplissy et al. (2016) obtained the "pure" binary nucleation rate at low temperature by excluding contaminated experiment runs based on the molecular identification of charged clusters using an APi-TOF. Our data, with the H_2SO_4 concentration in the nucleation zone ranged from $1.75 \times 10^{10}\,cm^{-3}$ to $3.19 \times 10^{10}\,cm^{-3}$ and corresponding *J* ranged from hundreds to thousands, is within the scope of previous overall results. The error bars of our data stand for uncertainties of the estimated H_2SO_4 concentration in the nucleation zone due to wall loss within ± 10 cm range of the nucleation zone.

Our results are also accompanied with a theoretical prediction of binary homogeneous nucleation calculated at 297K and 30% RH according to the parameterization suggested by Määttänen et al. (2018) The slope of experimental data is comparable to the theoretical prediction, and the experimental data are about one order of magnitude less than suggested by the theoretical prediction, which uses a model relying on thermodynamically consistent classical nucleation theory normalized with quantum chemical data on sulfuric acid hydration and on experimental data for vapor pressures **with** wider temperature and sulfuric acid concentration ranges than those of Vehkamäki et al. (2002) Though our H_2SO_4-H_2O nucleation results are most consistent with the parameterization, the possible trace-level contaminants arise from the carrier gas itself or simply surfaces in the experimental system may overestimate the experimental outcomes and particle detector with a certain size cutoff may pull back some.

3.2. CH_2O addition

3.2.1. Variation of SA at constant RH

Fig. 6 shows the nucleation rates as a function of $[H_2SO_4]_{NZ}$ for CH_2O additions of 0.31, 0.62, and 2.40 ppbv (± 50%), respectively, at 30% RH. The amount of CH_2O added was held steady for each set of measurements. Clearly, the number of particles increased but not obvious after addition of CH_2O. The enhancement factors (EF) are about 1.4, 1.9 and 2.2 at the CH_2O concentration of 0.31, 0.62 and 2.40 ppbv respectively. In comparison to the methylamine, where millionfold of EF were observed at hundred pptv level under similar conditions (RH = 27%, T = 296 K, $[H_2SO_4] = 10^9\,cm^{-3}$) by Zollner et al. (2012). CH_2O is a very weak particle formation partner with SA. Individual power law fits to these data show dependencies upon SA that scatter

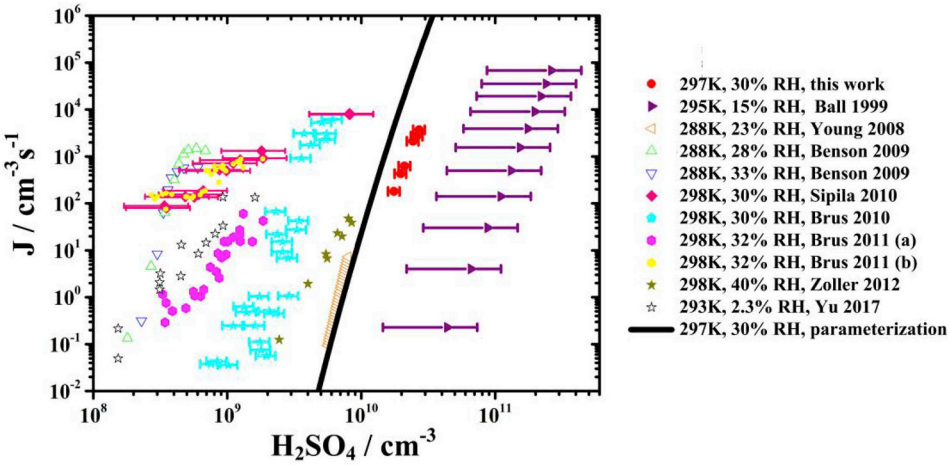

Fig. 5. A comparison of this work with the prediction and previous flow tube studies of H_2SO_4-H_2O nucleation where nucleation rate *J* is plotted against concentration of H_2SO_4. Those studies with solid symbols are results using H_2SO_4 vapor from sulfuric acid solutions entrained in a flow of gas (bulk) while those with hollow symbols use photo-oxidation of SO_2 as a source of H_2SO_4. Brus et al., 2011 (a) and Brus et al., 2011 (b) are the results from ultrafine CPC and PSM detection, respectively.

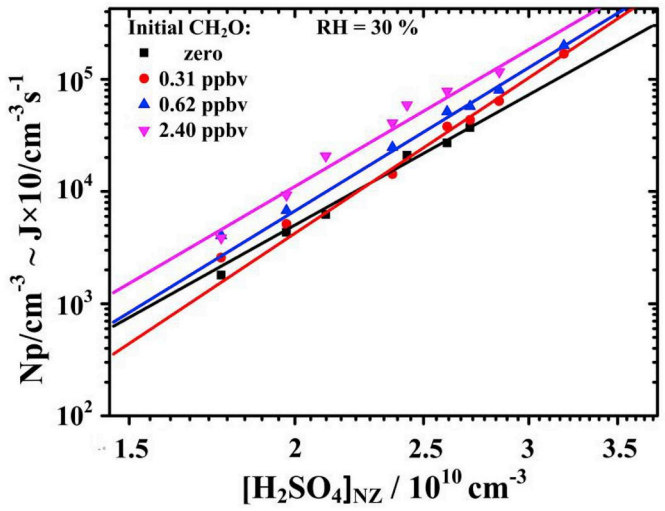

Fig. 6. *Np* or *J* plotted versus $[H_2SO_4]_{NZ}$ at three constant CH_2O concentrations. Value for the H_2SO_4-H_2O system is also shown in the plots. $[H_2SO_4]_{NZ}$ uncertainty was estimated to be ± 1.6% due to wall loss within ± 10 cm range of the nucleation zone.

from 6.92 to 7.86 with an average of 7.34, which is slightly larger than the SA power dependency of 6.59 for the H_2SO_4-H_2O system at 30% RH.

Fig. 7 shows corresponding particle size distributions for $[SA]_{NZ}$ of 1.76×10^{10} (a), 1.97×10^{10} (b), 2.37×10^{10} (c), 2.60×10^{10} (d), and $2.85 \times 10^{10}\,cm^{-3}$ (e) at 30% RH and different formaldehyde levels. Diameters of particles increased with increasing $[SA]_{NZ}$ at any formaldehyde level added in this study. Formaldehyde promoted growth with less and less obvious enhancement as formaldehyde concentration increases, and diameters of particles even decreased slightly when formaldehyde concentration increased up to 2.40 ppbv. This decrease may be attributed to the instability of the formaldehyde-related particles, which return smaller through evaporation as evaporation rate calculation in "Kinetics Model Calculations" section supports this explanation.

3.2.2. Variation of RH at constant SA

The effect of water was further investigated by monitoring particle formation as a function of RH. Fig. 8 shows the number concentrations of new particles formed when $1.97 \times 10^{10}\,cm^{-3}$ and $2.60 \times 10^{10}\,cm^{-3}$ of SA reacts with H_2O and/or CH_2O (2.4 ppbv). No particle formed only CH_2O and SA without the presence of water vapor. With $[SA]_{NZ}$ of $2.60 \times 10^{10}\,cm^{-3}$, the particle number concentration increases but is still only about one hundred particles cm^{-3}, which may be due to the experimental residue or background that instrument measured. Thus, the H_2SO_4-CH_2O combination does not efficiently form particle, the presence of water vapor is required.

Clearly, the data in Fig. 8 show the particle concentrations from SA, CH_2O and H_2O increase with increasing RH. At different RH cases, the CH_2O all weakly promotes the new particle formation due to the small promotion factors. With an estimate of $[SA]_{NZ} = 1.97 \times 10^{10}\,cm^{-3}$ and $2.60 \times 10^{10}\,cm^{-3}$, the EF changes from ~2 to ~4 when RH in the range of 20%–50%. Here, the experimental power dependencies of *J* on RH, obtained from variation of *Np* with RH, were 2.7 and 3.8, respectively, which is smaller than ~6 in the H_2SO_4-H_2O system (Zollner et al., 2012). There are more previous results in the SI.

Particle size distributions as a function of RH at 2.40 ppbv of formaldehyde for $[SA]_{NZ}$ of 1.97×10^{10} and $2.60 \times 10^{10}\,cm^{-3}$ are shown in Fig. 9. The particle diameters also kept increasing with increasing RH under these two sulfuric acid concentrations, reaching to 8.97 ± 25% nm at 50% RH from 8.25 ± 30% nm at 20% RH and reaching to 13.15 ± 20% nm at 48% RH from 9.89 ± 25% nm at 20% RH, respectively. These trends indicted that water not only promotes the number of particles formation but also grows small particles into diameters that be detected. Sulfuric acid can even evaporate from particles or be unable to contribute to their growth for conditions characterized by low relative humility, relatively high temperatures and weak sources of NH_3 and SO_2 (Tsagkogeorgas et al., 2017). Thus, water vapor is essential for particles formation in the CH_2O-H_2SO_4 system, which is consistent with following thermodynamic result.

3.3. Kinetics Model Calculations

Cluster formation energies of $(CH_2O)_l(H_2SO_4)_m$ (l = 0–3, m = 0–3, $l + m > 1$) $(H_2SO_4)_m(H_2O)_n$ (m = 0–3, n = 1–3, $m + n > 1$) and $(CH_2O)_l(H_2O)_n$ (l = 1–3, n = 1–3) clusters obtained at the PW91PW91/6–311 + + G(3df, 3pd) level of theory are presented in Table 1. The formation Gibbs free energy of $(CH_2O)(H_2SO_4)$ is $-1.15\,kcal\,mol^{-1}$, which is much smaller than those determined for the reactions between H_2SO_4 and H_2O/H_2SO_4. In addition, the combination of CH_2O and H_2O cannot form cluster. CH_2O may have negligible capability to form cluster with sulfuric acid and water in the early stages of new particle formation. Cluster formation energies of $(CH_2O)_l(H_2SO_4)m(H_2O)n$ (l = 1–3, m = 1–3, n = 1–3) clusters are shown in Table S3 in the SI. According to formation Gibbs free energies, all the formation of hydrated $(CH_2O)_l(H_2SO_4)m$ (l = 1–3, m = 1–3) clusters are thermodynamically favorable, while the formation of non-hydrated $(CH_2O)(H_2SO_4)m$ (m = 1–3) clusters are not easy and even impossible for clusters containing more CH_2O molecules. Thus, the collision of individual formaldehyde molecules to existing clusters may be detrimental to cluster growth.

In order to further determine whether the cluster can grow at 297 K and characterize the reaction mechanism of SA binding with CH_2O, the main cluster growth flux was subsequently obtained. Table 2 shows the evaporation rate, cluster growth flux and growth flux ratio, which determines the reaction channel, simulated for SA binding with CH_2O in the 3 × 3 size box (A: SA; B: CH_2O) under the condition of T = 297 K, RH = 30%, $[SA] = 2.60 \times 10^{10}\,cm^{-3}$ and $[CH_2O] = 5.93 \times 10^{10}\,cm^{-3}$ (2.40 ppbv). Although the calculated formation Gibbs free energy of 3A.3B cluster is $-9.15\,kcal\,mol^{-1}$, as shown in Table 1, the negative growth flux of 3A.3B cluster indicates that there is almost no 3A.3B cluster in the equilibrium condition. For 3A.2B cluster, only 0.2% form through the path $1A.\,2B + 2A \rightarrow 3A.\,2B$, however, 1A.2B cluster has no channel to form only by the evaporation of a CH_2O molecule from 1A.3B cluster or 2A.1B cluster from 3A.3B cluster. For 2A.3B cluster, 44% form through the path $1A.\,3B + A \rightarrow 2A.\,3B$, however, 1A.3B cluster has no channel to form similar to 1A.2B cluster; 0.01% form through the path $1A.\,2B + 1A.\,1B \rightarrow 2A.\,3B$, however, 1A.1B cluster also has no channel to form. By similar analysis, no 3A.1B, 2A.2B, 2A.1B, 3A, 3B and 1A.1B cluster exist in the equilibrium condition, too. In conclusion, there is no nucleation and further growth path for CH_2O with SA at the presence of water. Coordinates of all optimized $(CH_2O)_l(H_2SO_4)_m(H_2O)_n$ (l = 1–3, m = 0–3, n = 0–3) clusters are presented in the SI.

3.4. Comparison between experiment and calculation

Detailed kinetics simulation proved that CH_2O almost cannot participate in nucleation with SA, but the formation rate obtained from experiment increased slightly compared to H_2SO_4-H_2O nucleation shown in Fig. 6. More particles in the experiment may not directly form from the nucleation of formaldehyde. β-hydroxycarbonyl of CH_2OHCHO and α, β-unsaturated carbonyl of CH_2CO, the derivatives of formaldehyde from aldol condensation and further dehydration, respectively, and $CH_2(OH)_2$ from formaldehyde aldol condensation (Barsanti and Pankow, 2004) could promote new particle formation by stabilizing sulfuric acid in the first steps of nucleation. It has just been proved theoretically that the products derived from hydration of

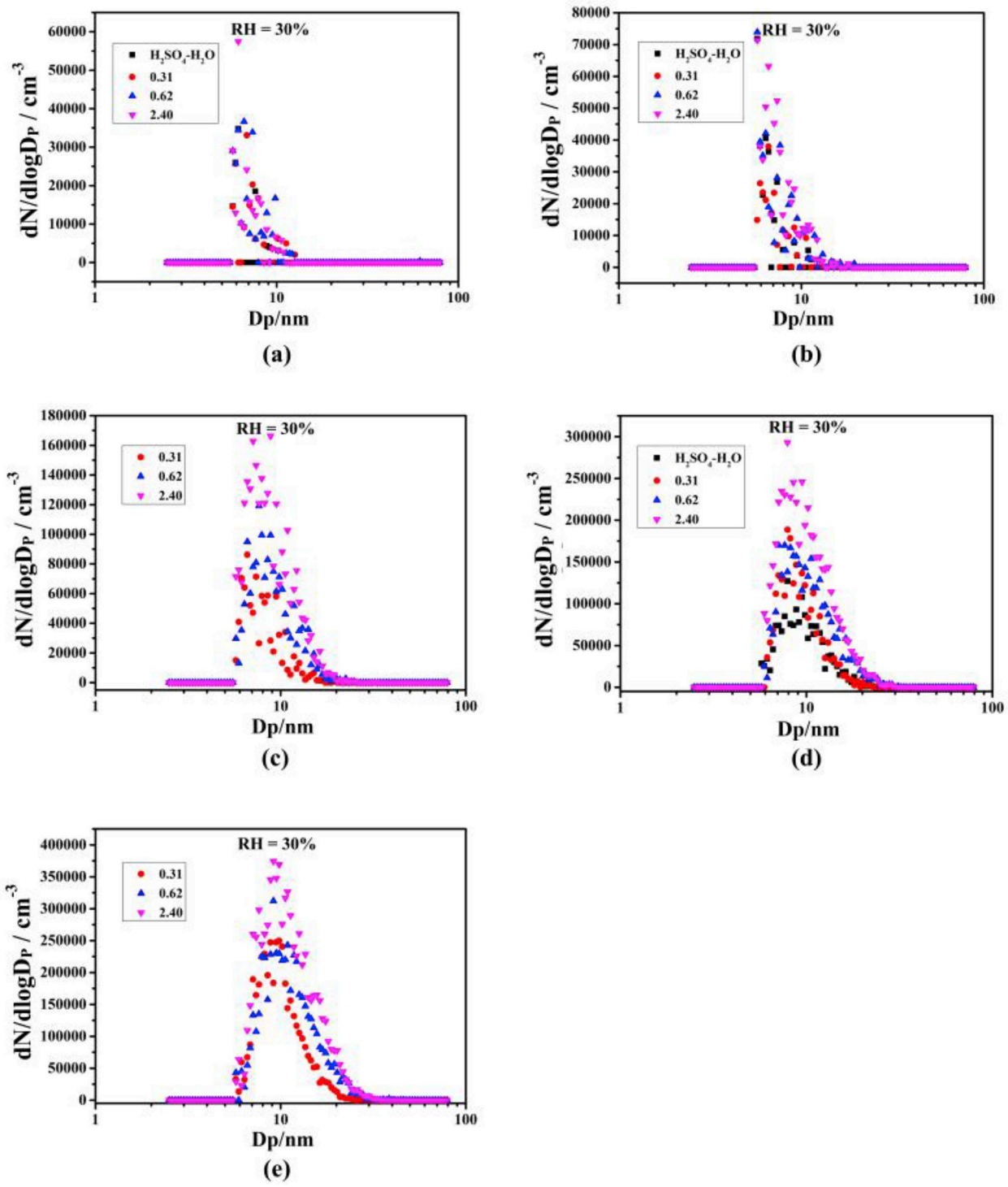

Fig. 7. Particle size distributions for $[SA]_{NZ}$ of 1.76×10^{10} (a), 1.97×10^{10} (b), 2.37×10^{10} (c), 2.60×10^{10} (d), and 2.85×10^{10} cm^{-3} (e) at 30% RH and different formaldehyde levels. The symbols across the plots are coded for formaldehyde levels in ppbv (approximately): circle, 0.31; triangle, 0.62; inverted triangle, 2.40; and the result for the H_2SO_4-H_2O system is shown with the square in the plots.

glyoxal and the products via aldol condensation of acetaldehyde could participate in the initial steps of atmospheric particle nucleation (Shi et al., 2018). The studies of formation pathways, steady-state concentrations and formation rates of these derivatives of CH_2O related clusters via quantum chemistry calculations and kinetics modeling are currently undergoing in our laboratory.

4. Conclusions

We have measured nucleation rates of particles produced from H_2SO_4-H_2O and CH_2O-H_2SO_4-H_2O in a laminar flow tube. Experiments were conducted in the RH ranging from 0.6% to 50% at the temperature of 297 K. The observed power dependency of H_2SO_4-H_2O nucleation rate on the concentration of SA was 6.59 at RH of 30%, and observed power dependency of CH_2O-H_2SO_4-H_2O nucleation rate on the concentration of SA was similar to this at an average of 7, while, power

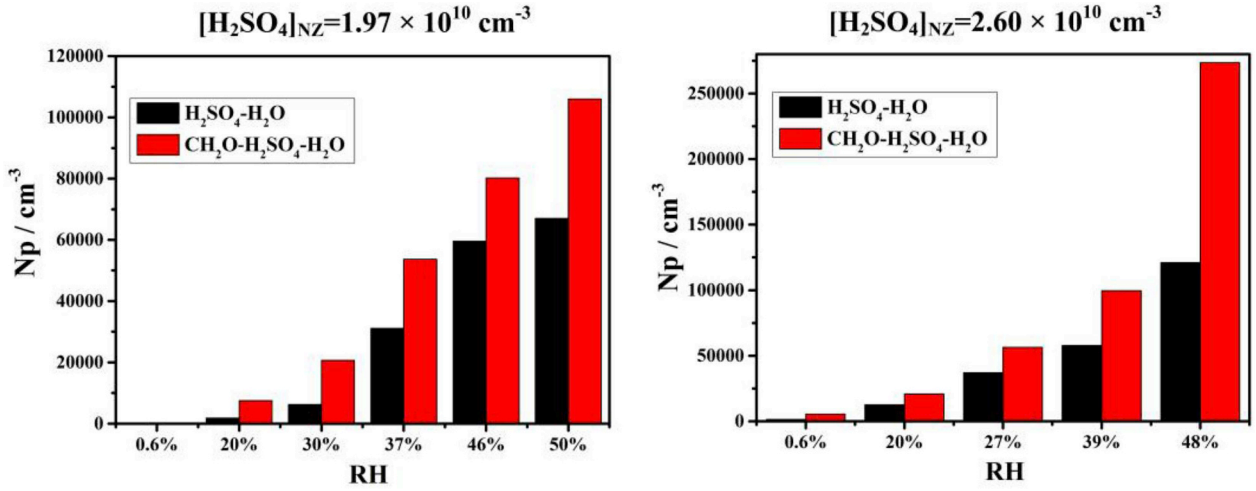

Fig. 8. *Np* versus RH at formaldehyde concentration of 2.40 ppbv for $[SA]_{NZ}$ of 1.97×10^{10} cm^{-3} and 2.60×10^{10} cm^{-3}. Value for the H_2SO_4-H_2O system is also shown in the plots.

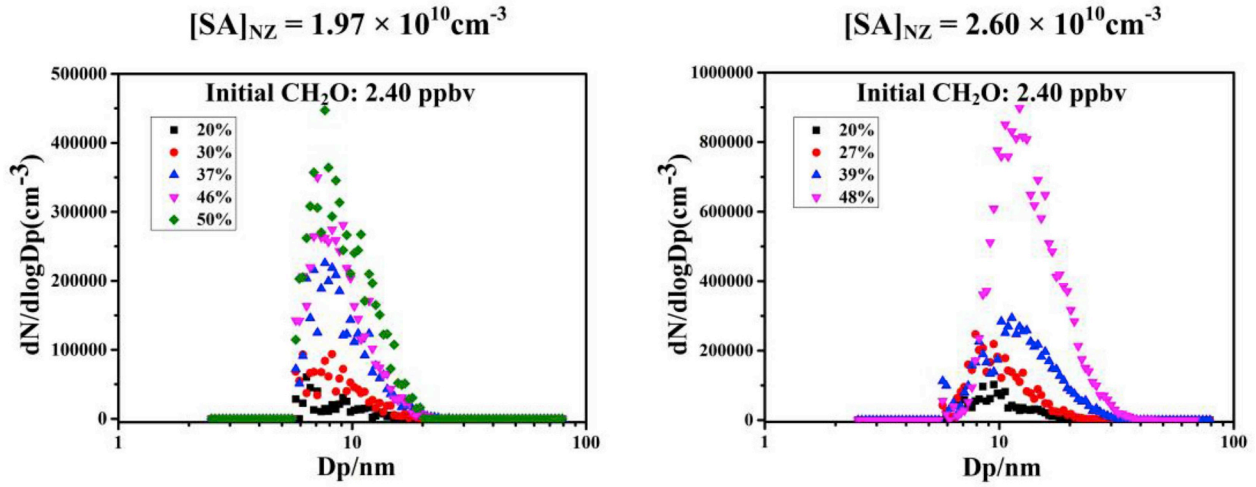

Fig. 9. Particle size distributions versus RH at 2.40 ppbv of formaldehyde for $[SA]_{NZ}$ of 1.97×10^{10} and 2.60×10^{10} cm^{-3}. The different symbols across the plots are coded for different RH levels.

Table 1
Electronic energies (ΔE_{elec}), Enthalpies (ΔH), Entropies (ΔS) and Gibbs free Energies (ΔG) of formation from monomers computed at the PW91/6–311 + + G(3df, 3pd) level of theory for $(CH_2O)_l(H_2SO_4)_m$ (l = 0–3, m = 0–3, $l + m > 1$) $(H_2SO_4)_m(H_2O)_n$ (m = 0–3, n = 1–3, $m + n > 1$) and $(CH_2O)_l(H_2O)_n$ (l = 1–3, n = 1–3) clusters. All values are at 298.15 K and 1atm reference pressure in kcal mol^{-1}.

Cluster	ΔE_{elec}	ΔH	ΔS	ΔG	Cluster	ΔE_{elec}	ΔH	ΔS	ΔG
$(CH_2O)_2$	−2.74	−3.05	−0.03	5.47	$(H_2SO_4)(H_2O)_3$	−33.28	−35.80	−0.10	−5.97
$(H_2SO_4)_2$	−16.41	−16.54	−0.04	−5.36	$(H_2SO_4)_2(H_2O)$	−29.60	−30.82	−0.07	−8.74
$(H_2O)_2$	−3.62	−4.17	−0.02	2.97	$(H_2SO_4)_2(H_2O)_2$	−41.10	−43.07	−0.11	−11.09
$(CH_2O)_3$	−5.65	−5.70	−0.05	10.34	$(H_2SO_4)_2(H_2O)_3$	−54.37	−57.39	−0.14	−14.16
$(H_2SO_4)_3$	−31.25	−31.73	−0.08	−8.02	$(H_2SO_4)_3(H_2O)$	−47.84	−49.21	−0.12	−14.30
$(H_2O)_3$	−12.49	−14.60	−0.06	3.91	$(H_2SO_4)_3(H_2O)_2$	−62.74	−65.54	−0.16	−18.55
$(CH_2O)(H_2SO_4)$	−10.21	−10.33	−0.01	−1.15	$(H_2SO_4)_3(H_2O)_3$	−75.26	−78.78	−0.19	−21.85
$(CH_2O)(H_2SO_4)_2$	−26.96	−27.20	−0.07	−7.14	$(CH_2O)(H_2O)$	−3.50	−3.76	−0.02	2.85
$(CH_2O)(H_2SO_4)_3$	−44.80	−45.59	−0.11	−11.62	$(CH_2O)(H_2O)_2$	−10.50	−11.73	−0.06	5.56
$(CH_2O)_2(H_2SO_4)$	−16.09	−16.88	−0.07	3.57	$(CH_2O)(H_2O)_3$	−18.97	−21.42	−0.09	6.81
$(CH_2O)_2(H_2SO_4)_2$	−41.38	−43.75	−0.12	−7.18	$(CH_2O)_2(H_2O)$	−7.70	−8.06	−0.05	7.61
$(CH_2O)_2(H_2SO_4)_3$	−52.72	−53.51	−0.15	−9.98	$(CH_2O)_2(H_2O)_2$	−16.22	−18.47	−0.10	10.96
$(CH_2O)_3(H_2SO_4)$	−32.20	−35.09	−0.12	0.53	$(CH_2O)_2(H_2O)_3$	−23.26	−25.61	−0.12	10.94
$(CH_2O)_3(H_2SO_4)_2$	−49.91	−52.90	−0.16	−6.58	$(CH_2O)_3(H_2O)$	−12.97	−14.80	−0.10	15.08
$(CH_2O)_3(H_2SO_4)_3$	−66.01	−69.40	−0.20	−9.15	$(CH_2O)_3(H_2O)_2$	−20.04	−22.32	−0.13	15.93
$(H_2SO_4)(H_2O)$	−11.05	−11.84	−0.03	−1.94	$(CH_2O)_3(H_2O)_3$	−28.04	−29.89	−0.15	14.32
$(H_2SO_4)(H_2O)_2$	−22.67	−24.38	−0.07	−4.49					

Table 2
The evaporation rate, cluster growth flux and growth flux ratio for SA binding with CH_2O in the 3*3 size box (A: SA; B: CH_2O). The cluster growth flux ratio means the percentage of one growth channel accounting for the total growth channels for one certain product cluster.

Product cluster	Evaporating molecule or cluster	Evaporation rate (s^{-1})	Cluster growth flux (m^{-3} s^{-1})	Growth flux ratio
3A.3B	3A	1.82e-02	−4.24e-10	2.24e-07
	3A.2B	4.03e+04	−3.64e-4	1.92e-01
	3A.1B	5.32e+01	−1.22e-6	6.45e-04
	2A.3B	7.10e+02	−1.99e-6	1.05e-03
	2A.2B	2.34e+02	−2.85e-6	1.51e-03
	2A.1B	1.79e+03	−2.24e-5	1.18e-02
	1A.3B	9.24e+05	−1.50e-03	7.93e-01
3A.2B	3A.1B	2.90e+11	−4.64e+05	9.96e-01
	3A	3.22e+07	−4.49e+02	9.64e-04
	2A.2B	1.77e+07	−6.48e+01	1.39e-04
	2A.1B	2.23e+08	−9.42e+02	2.02e-03
	1A.2B	1.56e+07	2.71e+02	5.82e-04
2A.3B	3B	1.73e+00	−2.22e-6	2.18e-09
	2A.1B	1.69e+05	−2.13e-01	2.09e-04
	2A.2B	9.67e+08	−5.60e+02	5.49e-01
	1A.3B	6.30e+08	4.60e+02	4.51e-01
	1A.2B	1.84e+05	1.55e-01	1.52e-04
3A.1B	3A	2.31e+10	−3.90e+14	9.99e-01
	2A.1B	2.23e+06	−6.27e+10	1.61e-04
	1A.1B	5.01e+05	−1.30e+10	3.33e-05
2A.2B	2B	1.12e+05	−2.01e+06	4.63e-05
	2A.1B	3.34e+10	−4.34e+10	9.99e-01
	1A.2B	4.82e+05	1.79e+07	4.12e-04
	1A.1B	8.59e+05	2.69e+07	6.19e-04
1A.3B	3B	7.83e-04	−5.70e-02	5.79e-09
	1A.1B	1.78e+01	−1.28e+03	1.30e-04
	1A.2B	8.30e+05	−9.84e+06	9.99e-01
2A.1B	2A	5.88e+08	−1.49e+18	9.99e-01
	1A.1B	6.37e+04	1.74e+15	1.17e-03
1A.2B	2B	5.31e+04	−8.45e+10	6.81e-04
	1A.1B	3.67e+09	−1.24e+14	9.99e-01
3A	2A	5.51e+04	−4.27e+17	1
3B	2B	4.80e+13	1.41e+08	1
1A.1B	1A	1.99e+09	−2.75e+22	1
2A	1A	2.46e+05	1.11e+23	1
2B	1B	1.23e+14	8.53e+23	1

dependency of CH_2O-H_2SO_4-H_2O nucleation rate on the concentration of H_2O was 3 ± 1. CH_2O, with a small EF, was found much less effective than amine at promoting nucleation with SA. Detailed kinetics simulation also proved that there is almost no path for CH_2O-H_2SO_4-relating clusters to form and grow. It is likely to conclude that CH_2O can be eliminated from direct nucleation considerations in the atmosphere. The derived information provides new insight into the impact of aldehydes on NPF. In the future, it is important to understand how the products of carbonyl compounds in the atmosphere participate in nucleation and how aldehydes affect surface film and surface changes, which further affect the new particle formation.

Notes

The author declares no competing financial interest.

Acknowledgments

This work was supported by the National Natural Science Foundation of China (Grant No. 21403244, 41775122, 21573241, 41605099, 41705097, 41705111, 41775112 and 41527808), the National Science Fund for Distinguished Young Scholars (Grant No. 41725019), Key Research Program of Frontier Science, CAS (Grant No. QYZDB-SSW-DQC031), The Key Research Program of the Chinese Academy of Sciences (Grant No. ZDRW-ZS-2016-4-3-6), the National Key Research and Development program (Grant No.2016YFC0202203 and 2016YFC0202703) and National Research Program for Key Issues in Air Pollution Control (DQGG0103).

Appendix A. Supplementary data

Supplementary data to this article can be found online at https://doi.org/10.1016/j.atmosenv.2018.12.057.

References

Almeida, J., Schobesberger, S., Kürten, A., Ortega, I.K., Kupiainen-Määttä, O., Praplan, A.P., et al., 2013. Molecular understanding of sulphuric acid–amine particle nucleation in the atmosphere. Nature 502, 359–363.
Alvarez-Idaboy, J.R., Mora-Diez, N., Boyd, R.J., Vivier-Bunge, A., 2001. On the importance of prereactive complexes in molecule − radical reactions: Hydrogen abstraction from aldehydes by oh. J. Am. Chem. Soc. 123 (9), 2018–2024.
Anderson, L.G., Lanning, J.A., Barrell, R., Miyagishima, J., Jones, R.H., Wolfe, P., 1996. Sources and sinks of formaldehyde and acetaldehyde: an analysis of denver's ambient concentration data. Atmos. Environ. 30 (12), 2113–2123.
Atkinson, R., 2000. Atmospheric chemistry of VOCs and NO_X. Atmos. Environ. 34 (12), 2063–2101.
Ball, S., Hanson, D., Eisele, F., McMurry, P., 1999. Laboratory studies of particle nucleation: initial results for H_2SO_4, H_2O, and NH_3 vapors. J. Geophys. Res. Atmos. 104 (D19), 23709–23718 1984–2012.
Barsanti, K.C., Pankow, J.F., 2004. Thermodynamics of the formation of atmospheric organic particulate matter by accretion reactions—part 1: aldehydes and ketones. Atmos. Environ. 38 (26), 4371–4382.
Benson, D.R., Erupe, M.E., Lee, S.-H., 2009. Laboratory-measured H_2SO_4-H_2O-NH_3 ternary homogeneous nucleation rates: initial observations. Geophys. Res. Lett. 36 (15), L15818.
Benson, D.R., Yu, J.H., Markovich, A., Lee, S.H., 2011. Ternary homogeneous nucleation of H_2SO_4, NH_3, and H_2O under conditions relevant to the lower troposphere. Atmos. Chem. Phys. 11 (10), 4755–4766.
Berndt, T., Sipilä, M., Stratmann, F., Petäjä, T., Vanhanen, J., Mikkilä, J., et al., 2014. Enhancement of atmospheric H_2SO_4/H_2O nucleation: organic oxidation products versus amines. Atmos. Chem. Phys. 14 (2), 751–764.
Brus, D., Hyvärinen, A.-P., Viisanen, Y., Kulmala, M., Lihavainen, H., 2010. Homogeneous nucleation of sulfuric acid and water mixture: experimental setup and first results. Atmos. Chem. Phys. 10, 2631–2641.
Brus, D., Neitola, K., Hyvärinen, A.P., Petäjä, T., Vanhanen, J., Sipilä, M., et al., 2011. Homogenous nucleation of sulfuric acid and water at close to atmospherically relevant conditions. Atmos. Chem. Phys. 11 (11), 5277–5287.
Brus, D., Škrabalová, L., Herrmann, E., Olenius, T., Trávníčková, T., Makkonen, U., Merikanto, J., 2017. Temperature-dependent diffusion of H_2SO_4 in air at atmospherically relevant conditions: laboratory measurements using laminar flow technique. Atmosphere 8 (12), 132.
Carbajo, P.G., Smith, S.C., Holloway, A.-L., Smith, C.A., Pope, F.D., Shallcross, D.E., Orr-Ewing, A.J., 2008. Ultraviolet photolysis of hcho: absolute hco quantum yields by direct detection of the hco radical photoproduct. J. Phys. Chem. A 112 (48), 12437–12448.
Duplissy, J., Merikanto, J., Franchin, A., Tsagkogeorgas, G., Kangasluoma, J., Wimmer, D., et al., 2016. Effect of ions on sulfuric acid-water binary particle formation: 2. Experimental data and comparison with qc-normalized classical nucleation theory. J. Geophys. Res. Atmos. 121 (4), 1752–1775.
Feilberg, K.L., D'Anna, B., Johnson, M.S., Nielsen, C.J., 2005. Relative tropospheric photolysis rates of HCHO, $H^{13}CHO$, $HCH^{18}O$, and DCDO measured at the european photoreactor facility. J. Phys. Chem. A 109 (37), 8314–8319.
Fried, A., Crawford, J., Olson, J., Walega, J., Potter, W., Wert, B., et al., 2003. Airborne tunable diode laser measurements of formaldehyde during TRACE-P: distributions and box model comparisons. J. Geophys. Res. Atmos. 108 (D20) (GTE).
Fried, A., McKeen, S., Sewell, S., Harder, J., Henry, B., Goldan, P., et al., 1997. Photochemistry of formaldehyde during the 1993 tropospheric oh photochemistry experiment. J. Geophys. Res. Atmos. 102 (D5), 6283–6296.
Glasoe, W.A., Volz, K., Panta, B., Freshour, N., Bachman, R., Hanson, D.R., et al., 2015. Sulfuric acid nucleation: an experimental study of the effect of seven bases. J. Geophys. Res. Atmos. 120 (5), 1933–1950.
Grosjean, D., 1982. Formaldehyde and other carbonyls in los angeles ambient air. Environ. Sci. Technol. 16 (5), 254–262.
Hak, C.I.P., Trick, S., Kern, C., Platt, U., Dommen, J., Ordó˜ nez, C., Prévôt, A.S.H., Junkermann, W., Astorga-Lloréns, C., Larsen, B.R., Mellqvist, J., Strandberg, A., Yu, Y., Galle, B., Kleffmann, J., Lörzer, J.C., Braathen, G.O., Volkamer, R., 2005. Intercomparison of four different in-situ techniques for ambient formaldehyde measurements in urban air. Atmos. Chem. Phys. 5, 2881–2900.

Hanson, D.R., Eisele, F., 2000. Diffusion of H_2SO_4 in humidified nitrogen: Hydrated H_2SO_4. J. Phys. Chem. A 104 (8), 1715–1719.
Hanson, D.R., Eisele, F.L., 2002. Measurement of prenucleation molecular clusters in the NH_3, H_2SO_4, H_2O system. J. Geophys. Res. Atmos. 107 (D12) AAC 10-11-AAC 10-18.
Hanson, D.R., McMurry, P.H., Jiang, J., Tanner, D., Huey, L.G., 2011. Ambient pressure proton transfer mass spectrometry: detection of amines and ammonia. Environ. Sci. Technol. 45 (20), 8881–8888.
Hazra, M.K., Francisco, J.S., Sinha, A., 2013. Gas phase hydrolysis of formaldehyde to form methanediol: impact of formic acid catalysis. J. Phys. Chem. A 117 (46), 11704–11710.
IPCC, 2013. In: Stocker, T.F. (Ed.), In Climate Change 2013: the Physical Science Basis. Contribution of Working Group I to the Fifth Assessment Report of the Intergovernmental Panel on Climate Change. Cambridge University Press.
Iraci, L.T., Tolbert, M.A., 1997. Heterogeneous interaction of formaldehyde with cold sulfuric acid: implications for the upper troposphere and lower stratosphere. J. Geophys. Res. Atmos. 102 (D13), 16099–16107.
Jacob, D.J., 2000. Heterogeneous chemistry and tropospheric ozone. Atoms. Environ. 34 (12–14), 2131–2159.
Jang, M., Carroll, B., Chandramouli, B., Kamens, R.M., 2003. Particle growth by acid-catalyzed heterogeneous reactions of organic carbonyls on preexisting aerosols. Environ. Sci. Technol. 37 (17), 3828–3837.
Jang, M., Czoschke, N.M., Northcross, A.L., 2005. Semiempirical model for organic aerosol growth by acid-catalyzed heterogeneous reactions of organic carbonyls. Environ. Sci. Technol. 39 (1), 164–174.
Jen, C.N., Bachman, R., Zhao, J., McMurry, P.H., Hanson, D.R., 2016. Diamine-sulfuric acid reactions are a potent source of new particle formation. Geophys. Res. Lett. 43 (2), 867–873.
Jen, C.N., McMurry, P.H., Hanson, D.R., 2014. Stabilization of sulfuric acid dimers by ammonia, methylamine, dimethylamine, and trimethylamine. J. Geophys. Res. Atmos. 119 (12), 7502–7514.
Jiang, S., Huang, T., Liu, Y.-R., Xu, K.-M., Zhang, Y., Lv, Y.-Z., Huang, W., 2014. Theoretical study of temperature dependence and Rayleigh scattering properties of chloride hydration clusters. Phys. Chem. Chem. Phys. 16 (36), 19241–19249.
Kürten, A., Bianchi, F., Almeida, J., Kupiainen-Määttä, O., Dunne, E.M., Duplissy, J., et al., 2016. Experimental particle formation rates spanning tropospheric sulfuric acid and ammonia abundances, ion production rates, and temperatures. J. Geophys. Res. Atmos. 121 (20) 12,377-12,400.
Kanawade, V.P., Benson, D.R., Lee, S.-H., 2012. Statistical analysis of 4-year observations of aerosol sizes in a semi-rural continental environment. Atmos. Environ. 59, 30–38.
Kanawade, V.P., Tripathi, S.N., Siingh, D., Gautam, A.S., Srivastava, A.K., Kamra, A.K., et al., 2014. Observations of new particle formation at two distinct indian sub-continental urban locations. Atmos. Environ. 96, 370–379.
Kangasluoma, J., Kuang, C., Wimmer, D., Rissanen, M.P., Lehtipalo, K., Ehn, M., et al., 2014. Sub-3 nm particle size and composition dependent response of a nano-cpc battery. Atmos. Meas. Tech. 7 (3), 689–700.
Kerminen, V.-M., Chen, X., Vakkari, V., Petäjä, T., Kulmala, M., Bianchi, F., 2018. Atmospheric new particle formation and growth: review of field observations. Environ. Res. Lett. 13 (10), 103003.
Kerminen, V.-M., Kulmala, M., 2002. Analytical formulae connecting the “real” and the “apparent” nucleation rate and the nuclei number concentration for atmospheric nucleation events. J. Atmos. Sci. 33 (4), 609–622.
Kirkby, J., Curtius, J., Almeida, J., Dunne, E., Duplissy, J., Ehrhart, S., et al., 2011. Role of sulphuric acid, ammonia and galactic cosmic rays in atmospheric aerosol nucleation. Nature 476, 429.
Kuang, C., McMurry, P.H., McCormick, A.V., Eisele, F.L., 2008. Dependence of nucleation rates on sulfuric acid vapor concentration in diverse atmospheric locations. J. Geophys. Res. 113 (D10).
Kulmala, M., Laaksonen, A., 1990. Binary nucleation of water–sulfuric acid system: comparison of classical theories with different H_2SO_4 saturation vapor pressures. J. Chem. Phys. 93 (1), 696–701.
Kulmala, M., Riipinen, I., Sipilä, M., Manninen, H.E., Petäjä, T., Junninen, H., et al., 2007. Toward direct measurement of atmospheric nucleation. Science 318 (5847), 89.
Kurtén, T., Loukonen, V., Vehkamäki, H., Kulmala, M., 2008. Amines are likely to enhance neutral and ion-induced sulfuric acid-water nucleation in the atmosphere more effectively than ammonia. Atmos. Chem. Phys. 8 (14), 4095–4103.
Kurtén, T., Torpo, L., Ding, C.-G., Vehkamäki, H., Sundberg, M.R., Laasonen, K., Kulmala, M., 2007. A density functional study on water-sulfuric acid-ammonia clusters and implications for atmospheric cluster formation. J. Geophys. Res. Atmos. 112 (D4).
Laaksonen, A., Kulmala, M., O'Dowd, C.D., Joutsensaari, J., Vaattovaara, P., Mikkonen, S., et al., 2008. The role of voc oxidation products in continental new particle formation. Atmos. Chem. Phys. 8, 2657–2665.
Li, G., Su, H., Li, X., Kuhn, U., Meusel, H., Hoffmann, T., et al., 2016. Uptake of gaseous formaldehyde by soil surfaces: a combination of adsorption/desorption equilibrium and chemical reactions. Atmos. Chem. Phys. 16 (15), 10299–10311.
Liu, F.-Y., Tan, X.-F., Long, Z.-W., Long, B., Zhang, W.-J., 2015. New insights in atmospheric acid-catalyzed gas phase hydrolysis of formaldehyde: a theoretical study. RSC Adv. 5 (42), 32941–32949.
Long, B., Tan, X.-F., Chang, C.-R., Zhao, W.-X., Long, Z.-W., Ren, D.-S., Zhang, W.-J., 2013. Theoretical studies on gas-phase reactions of sulfuric acid catalyzed hydrolysis of formaldehyde and formaldehyde with sulfuric acid and H_2SO_4···H_2O complex. J. Phys. Chem. A 117 (24), 5106–5116.
Määttänen, A., Merikanto, J., Henschel, H., Duplissy, J., Makkonen, R., Ortega, I.K., Vehkamäki, H., 2018. New parameterizations for neutral and ion-induced sulfuric acid-water particle formation in nucleation and kinetic regimes. J. Geophys. Res. Atmos. 123 (2), 1269–1296.
McGrath, M.J., Olenius, T., Ortega, I.K., Loukonen, V., Paasonen, P., Kurtén, T., et al., 2012. Atmospheric cluster dynamics code: a flexible method for solution of the birth-death equations. Atmos. Chem. Phys. 12 (5), 2345–2355.
Merikanto, J., Duplissy, J., Määttänen, A., Henschel, H., Donahue, N.M., Brus, D., et al., 2016. Effect of ions on sulfuric acid-water binary particle formation: 1. Theory for kinetic- and nucleation-type particle formation and atmospheric implications. J. Geophys. Res. Atmos. 121 (4), 1736–1751.
Merikanto, J., Napari, I., Vehkamäki, H., Anttila, T., Kulmala, M., 2007. New parameterization of sulfuric acid-ammonia-water ternary nucleation rates at tropospheric conditions. J. Geophys. Res. 112 (D15).
Metzger, A., Verheggen, B., Dommen, J., Duplissy, J., Prevot, A.S.H., Weingartner, E., et al., 2010. Evidence for the role of organics in aerosol particle formation under atmospheric conditions. Proc. Natl. Acad. Sci. U.S.A. 107 (15), 6646–6651.
Nadykto, A.B., Du, H., Yu, F., 2007. Quantum dft and df–dft study of vibrational spectra of sulfuric acid, sulfuric acid monohydrate, formic acid and its cyclic dimer. Vib. Spectrosc. 44 (2), 286–296.
Nadykto, A.B., Yu, F., 2007. Strong hydrogen bonding between atmospheric nucleation precursors and common organics. Chem. Phys. Lett. 435 (1), 14–18.
Nadykto, A.B., Yu, F., Herb, J., 2008. Towards understanding the sign preference in binary atmospheric nucleation. Phys. Chem. Chem. Phys. 10 (47), 7073–7078.
Nadykto, A.B., Yu, F., Jakovleva, M.V., Herb, J., Xu, Y., 2011. Amines in the earth's atmosphere: a density functional theory study of the thermochemistry of pre-nucleation clusters. Entropy 13 (2), 554–569.
Neitola, K., Brus, D., Makkonen, U., Sipilä, M., Mauldin Iii, R.L., Sarnela, N., et al., 2015. Total sulfate vs. Sulfuric acid monomer concenterations in nucleation studies. Atmos. Chem. Phys. 15 (6), 3429–3443.
Nel, A., 2005. Air pollution-related illness: effects of particles. Science 308 (5723), 804–806.
Oberdörster, G., Ferin, J., Gelein, R., Soderholm, S.C., Finkelstein, J., 1992. Role of the alveolar macrophage in lung injury: studies with ultrafine particles. Environ. Health Perspect. 97, 193–199.
Olenius, T., Kupiainen-Määttä, O., Ortega, I.K., Kurtén, T., Vehkamäki, H., 2013. Free energy barrier in the growth of sulfuric acid–ammonia and sulfuric acid—dimethylamine clusters. J. Chem. Phys. 139 (8), 084312.
Ortega, I.K., Kupiainen, O., Kurtén, T., Olenius, T., Wilkman, O., McGrath, M.J., et al., 2012. From quantum chemical formation free energies to evaporation rates. Atmos. Chem. Phys. 12 (1), 225–235.
Possanzini, M., Palo, V.D., Cecinato, A., 2002. Sources and photodecomposition of formaldehyde and acetaldehyde in rome ambient air. Atmos. Environ. 36 (19), 3195–3201.
Qiu, C., Zhang, R., 2013. Multiphase chemistry of atmospheric amines. Phys. Chem. Chem. Phys. 15 (16), 5738–5752.
Riccobono, F., Schobesberger, S., Scott, C.E., Dommen, J., Ortega, I.K., Rondo, L., et al., 2014. Oxidation products of biogenic emissions contribute to nucleation of atmospheric particles. Science 344 (6185), 717–721.
Rosenboum, E.J., 1941. The mathematical theory of non-uniform gases (chapman, s.; cowling, t. G.). J. Chem. Educ. 18 (1), 48.
Schobesberger, S., Junninen, H., Bianchi, F., Lonn, G., Ehn, M., Lehtipalo, K., et al., 2013. Molecular understanding of atmospheric particle formation from sulfuric acid and large oxidized organic molecules. Proc. Natl. Acad. Sci. U.S.A. 110 (43), 17223–17228.
Shi, X., Zhang, R., Sun, Y., Xu, F., Zhang, Q., Wang, W., 2018. A density functional theory study of aldehydes and their atmospheric products participating in nucleation. Phys. Chem. Chem. Phys. 20 (2), 1005–1011.
Sipilä, M., Tuukka Petäjä, T.B., Brus, D., Vanhanen, J., Stratmann, F., P, J., Mauldin III, Roy L., Hyvärinen, Antti-Pekka, Heikki Lihavainen, M.K., 2010. The role of sulfuric acid in atmospheric nucleation. Science 327, 1243–1246.
Skrabalova, L., Brus, D., Anttila, T., Zdimal, V., Lihavainen, H., 2014. Growth of sulphuric acid nanoparticles under wet and dry conditions. Atmos. Chem. Phys. 14 (12), 6461–6475.
Tie, X., Brasseur, G., Emmons, L., Horowitz, L., Kinnison, D., 2001. Effects of aerosols on tropospheric oxidants: a global model study. J. Geophys. Res. Atmos. 106 (D19), 22931–22964.
Tsagkogeorgas, G., Roldin, P., Duplissy, J., Rondo, L., Tröstl, J., Slowik, J.G., et al., 2017. Evaporation of sulfate aerosols at low relative humidity. Atmos. Chem. Phys. 17 (14), 8923–8938.
Vanhanen, J., Mikkilä, J., Lehtipalo, K., Sipilä, M., Manninen, H.E., Siivola, E., et al., 2011. Particle size magnifier for nano-cn detection. Aerosol Sci. Technol. 45 (4), 533–542.
Vehkamäki, H., Kulmala, M., Napari, I., Lehtinen, K.E.J., Timmreck, C., Noppel, M., Laaksonen, A., 2002. An improved parameterization for sulfuric acid–water nucleation rates for tropospheric and stratospheric conditions. J. Geophys. Res. Atmos. 107 (D22) AAC 3-1-AAC 3-10.
Wagner, V., von Glasow, R., Fischer, H., Crutzen, P.J., 2002. Are CH_2O measurements in the marine boundary layer suitable for testing the current understanding of ch4 photooxidation?: a model study. J. Geophys. Res. Atmos. 107 (D3) ACH 3-1-ACH 3-14.
Wang, C.-Y., Jiang, S., Liu, Y.-R., Wen, H., Wang, Z.-Q., Han, Y.-J., et al., 2018. Synergistic effect of ammonia and methylamine on nucleation in the earth's atmosphere. A theoretical study. J. Phys. Chem. A 122, 3470–3479.
Wang, X., Wang, H., Wang, S., 2010. Ambient formaldehyde and its contributing factor to ozone and oh radical in a rural area. Atmos. Environ. 44 (17), 2074–2078.
Weber, R.J., Marti, J.J., McMurry, P.H., Eisele, F.L., Tanner, D.J., Jefferson, A., 1996. Measured atmospheric new particle formation rates: implications for nucleation mechanisms. Chem. Eng. Commun. 151 (1), 53–64.
Wen, H., Huang, T., Wang, C.-Y., Peng, X.-Q., Jiang, S., Liu, Y.-R., Huang, W., 2018. A study on the microscopic mechanism of methanesulfonic acid-promoted binary

nucleation of sulfuric acid and water. Atmos. Environ. 191, 214–226.
Yao, L., Garmash, O., Bianchi, F., Zheng, J., Yan, C., Kontkanen, J., et al., 2018. Atmospheric new particle formation from sulfuric acid and amines in a Chinese megacity. Science 361 (6399), 278–281.
Young, L.H., Benson, D.R., Kameel, F.R., Pierce, J.R., Junninen, H., Kulmala, M., Lee, S.-H., 2008. Laboratory studies of H_2SO_4/H_2O binary homogeneous nucleation from the SO_2+OH reaction: evaluation of the experimental setup and preliminary results. Atmos. Chem. Phys. 8, 4997–5016.
Yu, H., Dai, L., Zhao, Y., Kanawade, V.P., Tripathi, S.N., Ge, X., et al., 2017. Laboratory observations of temperature and humidity dependencies of nucleation and growth rates of sub-3nm particles. J. Geophys. Res. Atmos. 122 (3), 1919–1929.
Zhang, R., Khalizov, A., Wang, L., Hu, M., Xu, W., 2012. Nucleation and growth of nanoparticles in the atmosphere. Chem. Rev. 112 (3), 1957–2011.
Zheng, J., Ma, Y., Chen, M., Zhang, Q., Wang, L., Khalizov, A.F., et al., 2015. Measurement of atmospheric amines and ammonia using the high resolution time-of-flight chemical ionization mass spectrometry. Atmos. Environ. 102, 249–259.
Zheng, J., Zhang, R., Garzón, J.P., Huertas, M.E., Levy, M., Ma, Y., et al., 2013. Measurements of formaldehyde at the u.S.–Mexico border during the cal-mex 2010 air quality study. Atmos. Environ. 70, 513–520.
Zhou, X., Lee, Y.-N., Newman, L., Chen, X., Mopper, K., 1996. Tropospheric formaldehyde concentration at the mauna loa observatory during the mauna loa observatory photochemistry experiment 2. J. Geophys. Res. Atmos. 101 (D9), 14711–14719.
Zimmerman, P.R., Chatfield, R.B., Fishman, J., Crutzen, P.J., Hanst, P.L., 1978. Estimates on the production of co and h2 from the oxidation of hydrocarbon emissions from vegetation. Geophys. Res. Lett. 5 (8), 679–682.
Zollner, J.H., Glasoe, W.A., Panta, B., Carlson, K.K., McMurry, P.H., Hanson, D.R., 2012. Sulfuric acid nucleation: power dependencies, variation with relative humidity, and effect of bases. Atmos. Chem. Phys. 12 (10), 4399–4411.